JOURNAL OF THE ROYAL SOCIETY Interface

rsif.royalsocietypublishing.org

Research

Cite this article: Loskill P, Puthoff J, Wilkinson M, Mecke K, Jacobs K, Autumn K. 2012 Macroscale adhesion of gecko setae reflects nanoscale differences in subsurface composition. J R Soc Interface 10: 20120587. http://dx.doi.org/10.1098/rsif.2012.0587

Received: 23 July 2012
Accepted: 28 August 2012

Subject Areas:
nanotechnology, biophysics, biomaterials

Keywords:
van der Waals forces, gecko adhesion, surface energy

Authors for correspondence:
Karin Jacobs
e-mail: k.jacobs@physik.uni-saarland.de
Kellar Autumn
e-mail: autumn@lclark.edu

Electronic supplementary material is available at http://dx.doi.org/10.1098/rsif.2012.0587 or via http://rsif.royalsocietypublishing.org.

Royal Society Publishing
Informing the science of the future

Macroscale adhesion of gecko setae reflects nanoscale differences in subsurface composition

Peter Loskill[1], Jonathan Puthoff[2], Matt Wilkinson[2], Klaus Mecke[3], Karin Jacobs[1] and Kellar Autumn[2]

[1]Experimental Physics, Saarland University, 66041 Saarbrücken, Germany
[2]Department of Biology, Lewis and Clark College, Portland, OR 97219, USA
[3]Institute for Theoretical Physics, Universität Erlangen-Nürnberg, 91058 Erlangen, Germany

Surface energies are commonly used to determine the adhesion forces between materials. However, the component of surface energy derived from long-range forces, such as van der Waals forces, depends on the material's structure below the outermost atomic layers. Previous theoretical results and indirect experimental evidence suggest that the van der Waals energies of subsurface layers will influence interfacial adhesion forces. We discovered that nanometre-scale differences in the oxide layer thickness of silicon wafers result in significant macroscale differences in the adhesion of isolated gecko setal arrays. Si/SiO_2 bilayer materials exhibited stronger adhesion when the SiO_2 layer is thin (approx. 2 nm). To further explore how layered materials influence adhesion, we functionalized similar substrates with an octadecyltrichlorosilane monolayer and again identified a significant influence of the SiO_2 layer thickness on adhesion. Our theoretical calculations describe how variation in the SiO_2 layer thickness produces differences in the van der Waals interaction potential, and these differences are reflected in the adhesion mechanics. Setal arrays used as tribological probes provide the first empirical evidence that the 'subsurface energy' of inhomogeneous materials influences the macroscopic surface forces.

1. Introduction

When describing adhesion between two materials, it is common to refer to the strength of the contribution of each material using their surface energies (γ_1 and γ_2), which are the extra free energies (per unit area) possessed by atoms at a surface relative to atoms in the bulk [1]. The well-known Dupré equation gives the work of adhesion $\Delta\gamma$, the energy required to separate the dissimilar materials, as $\Delta\gamma = \gamma_1 + \gamma_2 - \gamma_{1,2}$, where $\gamma_{1,2}$ is the interfacial energy of the two contacting surfaces. The surface energy of solids typically cannot be measured directly and is usually estimated from liquid drop contact angle measurements [2]. The surface energy is largely a property of the outermost atomic layers (1 nm deep), yet van der Waals (vdW) forces act over distances greater than 1 nm in many cases [3–5]. Thin industrial coatings such as adhesion promoters, self-assembled monolayers of thiols or silanes as well as photoresists are also in the range of a few nanometres. The vdW forces of the underlying material should—theoretically—reach through the thin layer and influence adhesion.

Previous experiments, indeed, identified a significant influence of the long-range component of the interaction potential on the dewetting of thin liquid films [6,7], their liquid front profiles [8,9] and the mesoscopic organization of magnetic nanocrystals [10]. Recently, a similar influence was detected on the adsorption kinetics of proteins [11–13] and the adhesion of bacteria [14]. These experiments used materials whose contribution to the potential had been tuned by means of surface stratification. In layered systems, the contributions of the

different materials can be tuned by modifying the layer thicknesses [15]. Early work by Israelachvili & Tabor [16] measured the forces between crossed cylinders, one of which was covered with a monolayer of stearic acid, and found that the resulting dispersion forces were sensitive to the presence of the surface layer at small separations, on the order of the layer thickness. An analogous effect will apply when two materials are brought into contact, and the layer thickness is varied. The question presents itself: can stratification be used to modify the macroscopic adhesion of materials?

To tackle this question, we used the gecko to probe adhesion and the underlying surface forces. Although the gecko is essentially a macroscopic 'object',[1] it makes use of intermolecular forces. The outstanding climbing ability of the gecko has impressed observers for hundreds of years, and its technical replication is an active area of research nowadays [18]. The key adaptation that provides this ability is the hierarchical structure of a gecko foot. The underside of each toe is divided into lamellar structures that terminate in arrays of densely packed hair-like protrusions, called seta [19,20]. Individual setae are bundles of β-keratin fibrils several hundred micrometres long [21]. These fibrils terminate in triangular, wedge-shaped pads about 150 nm wide at the tip, called spatulae. As a consequence of this hierarchical structure, the setal arrays have an overall compliance that allows them to closely conform to rough surfaces [22]. The nanoscopic contacts that are established at the spatular tips produce considerable overall adhesion on virtually any surface by vdW interactions [23–25]. These structures are positioned at the correct scale to establish uniform, single-asperity contacts on substrates with limited roughness below 100 nm.

In this study, we measured the adhesion of isolated gecko setal arrays to substrates that differed only in their subsurface composition: we used Si wafer surface with a native ('N', 1.7(3) nm thick) oxide layer and surfaces with a thermally grown ('T', 151(1) nm thick) amorphous SiO_2 layer. In addition, we functionalized T- and N-type wafers with an octadecyltrichlorosilane (OTS) self-assembled monolayer. The OTS monolayer has optical properties that are similar to those of SiO_2, but is strongly hydrophobic. By using this set of substrates, we characterize the influence of the subsurface composition independent of surface interactions, because the latter are identical within the substrate pairs featuring the same surface chemistry [26]. A comparison between the substrates featuring different chemistries, however, is not the aim of this study, because hydrophilic and hydrophobic substrates differ in short-range interactions, the characterization of which is not simply covered by one parameter (e.g. the surface energy). Comparing, however, pairs of wafers with identical short-range forces, yet different thicknesses of the surface layers, will reveal the impact of vdW interaction and allow for a theoretical description. Our tribological probe was an isolated setal array from a species of tropical gecko (*Gekko gecko*; figure 1). Although the forces between each nano-hair and the surface are slight, the scaling of forces implied by the 'contact-splitting effect' [24,27] yields considerable adhesion when the number of hairs packed on the array is large.

1.1. Surface forces for layered media

We address the question of whether or not subsurface differences influence the adhesion between bodies by calculating the surface interaction potential and the resulting effect on

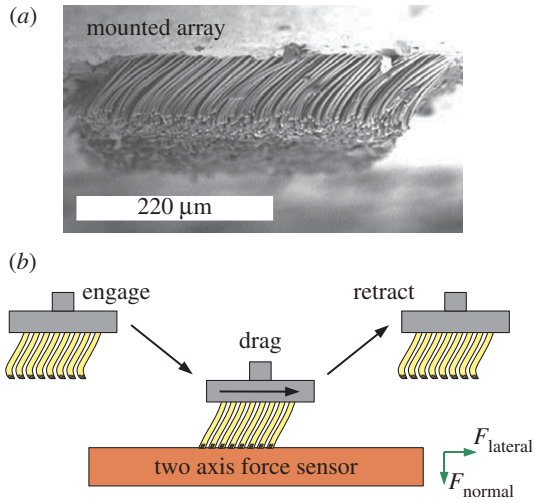

Figure 1. (*a*) A scanning electron microscope image of a mounted setal array. (*b*) Schematic of the test set-up for determining the adhesion (normal) forces and friction (lateral) forces between an array and a substrate. (Online version in colour.)

adhesion in a simple model system. Qualitatively, we expect a larger adhesion force between a probe object and a wafer with a thin oxide layer: because Si possesses a higher index of refraction and a higher polarizability than SiO_2, the vdW interactions between a probe object and Si are stronger than between a probe object and SiO_2 [3]. The probe will 'feel' the subsurface bulk silicon more in a type N wafer than in a type T wafer. The interaction ϕ between two bodies at a distance x can be described by a modified Lennard–Jones-type potential consisting of a short-range (SR) part and a long-range (LR) part

$$\begin{aligned}\phi(x) &= \phi_{SR}(x) + \phi_{LR}(x)\\ &= \frac{C_{SR}}{x^m} - C_{C,E}\cdot\Theta(x_0 - x) - \frac{C_{LR}}{x^n},\end{aligned} \tag{1.1}$$

where C_{SR} and C_{LR} are constants and m is typically chosen to be $n + 6$ to represent the powerful repulsion between overlapping electron clouds. Short-range chemical or entropic forces that act only at some separation x_0 are approximated by a Heaviside step function $\Theta(x)$ with constant strength $C_{C,E}$.

In the absence of charges, the LR part is determined exclusively by the vdW interactions ϕ_{vdW}. For two infinite planes interacting[2] through a medium M, the exponent $n = 2$ and the interaction energy per unit area is given by $\phi_{LR}(x) = \phi_{vdW}(x) = -A_{i/M/j}/12\pi x^2$, where $A_{i/M/j}$ is the Hamaker constant for the interaction of two materials i and j through a medium (M) and can be derived from the optical properties of the materials using the Lifschitz approach [3,28,29]. In the case of a probe material (P) interacting with a substrate that consists of a bulk material (L2) and a thin coating (L1) of thickness d, the vdW part of the interface potential can be modified as [6,7]

$$\phi_{vdW}(x) = -\frac{1}{12\pi}\left[\frac{A_{P/M/L1}}{x^2} + \frac{A_{P/M/L2} - A_{P/M/L1}}{(x+d)^2}\right]. \tag{1.2}$$

Hence, the relative contribution of different layers of an inhomogeneous substrate to the total LR vdW potential can be tuned by varying the thickness d of the layer L1. The second term in equation (1.2), incorporating the contribution from the lower layer, might be thought of as the 'subsurface energy' of the system. In the following, we use this term for energies that arise from vdW contributions to the interface potential owing to a variable subsurface composition.

2. Material and methods

2.1. Adhesion performance testing

We measured the tribological performance of the mounted setal arrays using a custom mechanical testing platform ('Robotoe') [30]. Robotoe incorporates a two-axis positioning stage (Aerotech, Pittsburg, PA, USA) and a piezoelectric load cell (Kistler, Amherst, NY, USA) with a resolution of 1.3 and 2.6 mN in shear and normal forces, respectively. The mounted array is attached to the terminal end of the force sensor assembly, and the layered Si/SiO_2/OTS substrates are held rigidly in a mount on the motion stage opposite the setal array specimen chuck. All of the components are enclosed in a controlled-environment chamber. During a test, the tips of the setal arrays are dragged across the substrate in a displacement-controlled motion designed to resemble a gecko's footfall [30] (cf. figure 1). Reported adhesion and friction values are taken from the force sensor readout during the steady-state portion of each test [31]. We can specify parameters such as the drag velocity v and the approach distance during the experiment, as well as the temperature and humidity in the chamber.

2.2. Preparation and cleaning of substrates

The silicon wafers were purchased from Si-Mat (Landsberg, Germany). We removed residues left over from the polishing process, as well as contaminants deposited by the atmosphere, by submerging the as-received wafers for 30 min in fresh 1 : 1 H_2SO_4(conc.)/H_2O_2 (30%) solution. The wafers were subsequently rinsed in boiling deionized water (DI) for 90 min, which was exchanged three times within that time. We produced a second pair of type T/type N substrates with different surface properties by hydrophobizing a series of cleaned wafers using self-assembling silane molecules with a CH_3 tailgroup (OTS, purchased from Sigma-Aldrich, Germany) following standard procedures [32,33]. All wafer types were characterized using atomic force microscopy, ellipsometry and water contact angle measurements (cf. table 2; further characterization data available in [13,34]). Immediately prior to the experiments, the substrates were cleaned by immersing them subsequently into ethanol and acetone (5 min each) in a ultrasonic bath and rinsing them for 30 min in boiling DI water.

2.3. Setal array collection and preparation

The setal arrays of *Gekko gecko* grow from lamellar strips of tissue on the ventral side of each toe. We collected entire arrays from live, unanaesthetized animals following the methods described in Autumn & Peattie [24]; the keratin backing layer to which the hairs are attached can be peeled off from the lamella easily. (The animal's loss of adhesive function in this digit is recovered at the next moult.) After some trimming, we affix the detached arrays to aluminium stubs, hairs facing upwards at their natural resting angle, with a thin layer of cyanoacrylate glue (cf. figure 1). These stubs are then mounted on the force sensor in Robotoe, the setal arrays facing the substrates mounted on the translation stage. The size of the arrays varies in the range of a few millimetres. The larger arrays were chosen for the experiments on the hydrophobic samples, the smaller ones for experiments on hydrophilic samples.

3. Results

3.1. Calculation of microscopic van der Waals potentials

The optical properties of Si and SiO_2 are well-known, but only limited data on the optical properties of β-keratin are available, and, to the authors' knowledge, no studies have been done on β-keratin from geckos. Furthermore, the constant C_{SR} in the repulsive part of equation (1.1) is hardly accessible, and so we cannot give rigorous theoretical values for the forces without some assumptions. We take the optical constants of β-keratin as those determined for horn keratin [35,36] (cf. table 1). We also assume that the repulsive constant C_{SR} and $C_{C,E}$ are independent of oxide layer thickness; this is a safe assumption because the surface properties of the substrates do not differ significantly (table 2). By using the indices of reflection and the dielectric constants of the involved materials (cf. table 1), the Hamaker constants were calculated to be $A_{Si} = 61.5\,k_BT$ and $A_{SiO_2} = 17.8\,k_BT$; confer chapter 11, eqn (11.13) of Israelachvili [3]. Inserting these values into equations (1.1) and (1.2) produces the potentials ϕ_N and ϕ_T in figure 2*a*. As expected from the qualitative considerations before, the global minimum in the interaction potential is lower for the type N than for the type T sample. For these potentials, we used $C_{SR} = 10^{-77}$ J m^6, a value that reflects the typical magnitude given in other experiments [6]. The term $C_{C,E}$, i. e. the chemical and entropic forces can be neglected in force differences because they would contribute—if significantly present at all—in the same way for type N and type T samples owing to their identical surface properties. Altogether, this results in maximal forces comparable to previous experimental studies [23]. The work of adhesion for these potentials is given by $\Delta\gamma = \phi(\infty) - \phi(x_0)$.

Table 1. Optical properties of the relevant materials [35–38].

	n	ε
β-keratin	1.56	20
SiO_2	1.46	3.9
Si	4.1	11.8
OTS	1.46	2

Avoiding all of the earlier-mentioned assumptions that especially concern the SR forces, it is instructive to evaluate the system in terms of LR vdW forces only. Of significant interest is the manner in which the vdW forces differ between the N and T substrates. This difference, on a per unit area basis, is

$$\Delta F(x) = F_N(x) - F_T(x) \propto \frac{A_{P/M/Si} - A_{P/M/SiO_2}}{(x+d)^3}. \tag{3.1}$$

This leads to a relative difference in vdW forces of

$$\Delta F_{Rel.}(x) = \frac{\Delta F(x)}{F_T(x)} = \frac{R_A}{(d/x+1)^3}, \tag{3.2}$$

where $R_A = A_{P/M/Si}/A_{P/M/SiO_2} - 1$ is the shifted ratio of the Hamaker constants. The parameter R_A is useful for comparing vdW force differences between substrates with different materials or structure. The relative difference in vdW forces on type T and type N wafers for different separations is shown in figure 2*b* whereby $R_A = 2.5$. Variation in the values of the refractive index and dielectric constant of β-keratin does not change these ratios significantly (see the electronic supplementary material).

3.2. Influence of the potentials ϕ_N and ϕ_T on adhesion forces

Adhesion between bodies involves more phenomena than just those represented by the interaction potential. For instance,

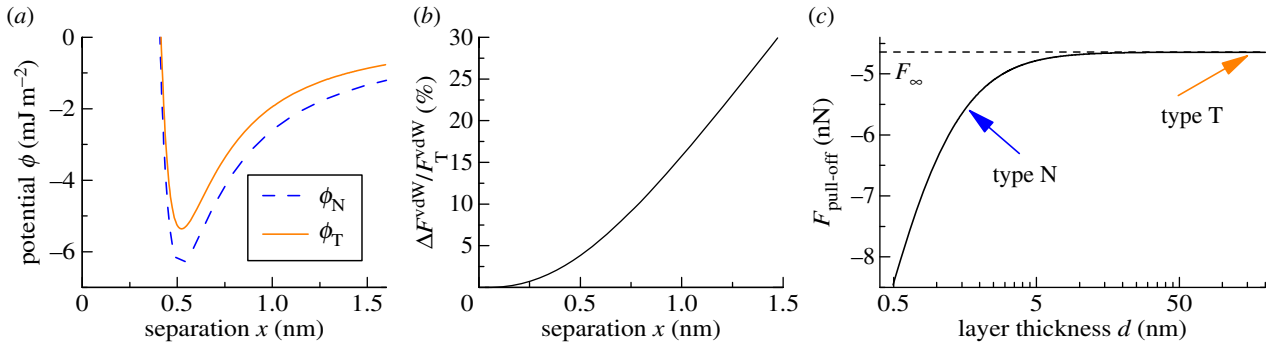

Figure 2. (*a*) Calculated effective interface potentials for the interaction between a keratin layer and a silicon wafer (type T and type N). The short-range constant was assumed as $C_{SR} = 1 \times 10^{-77}$ J m^6, resulting in maximal forces of $F_{max} \approx 10^{-2}$ nN nm^{-2} . (*b*) Relative difference in vdW forces on type T and type N wafers as determined using equation (3.2). (*c*) Estimated pull-off forces for a β-keratin sphere of radius $R = 150$ nm on a Si/SiO_2 bilayer material with layer thickness d making use of equation (3.4). (Online version in colour.)

Table 2. Surface properties of the substrates used in this study: root mean square (r.m.s.) roughness, advancing (adv.) and receding (rec.) water contact angle, surface energy γ and Lifshitz–van der Waals γ^{LW} and Lewis acid–base γ^{AB} components obtained from contact angles of three different liquids [39]. The number in brackets gives the error bar of the last digit.

	r.m.s. (nm)	γ (mJ m^{-2})	γ^{LW} (mJ m^{-2})	γ^{AB} (mJ m^{-2})	Θ_{adv} (°)	Θ_{rec} (°)
OTS T	0.19(3)	24(1)	24(1)	0	111(3)	103(4)
OTS N	0.17(0)	24(1)	24(1)	0	111(2)	103(2)
SiO_2 T	0.13(3)	63(1)	43(1)	20(1)	5(2)	complete wetting
SiO_2 N	0.09(2)	64(1)	43(1)	21(1)	7(2)	complete wetting

the separation of adhered structures is also influenced by the mechanical properties of the materials involved. More inclusive mechanical pictures of contact and adhesion include the Johnson–Kendall–Roberts (JKR) theory [40] and the Derjaguin–Muller–Toparov (DMT) theory [41] of contacting spheres. These models make specific predictions of the contact areas and pull-off forces for a number of different simple contact geometries (sphere/sphere, sphere/plane) based on materials' properties and surface interactions.

We investigate the influence of the interaction potential of equation (1.2) on the adhesion of a sphere of radius R to a plane using the same approach as these theories, but it is important to note that (i) equation (1.2) was derived for two facing half-spaces of material and (ii) the scaling of the adhesion forces will not be exactly linear with the changes in γ or F. We address these issues by transforming the interaction potential ϕ to a new form V amenable for contact between curved bodies using the Derjaguin approximation [42]. For contact between a body of principal curvatures κ_1, κ_2 and a plane, this gives

$$V(l) = -\frac{\alpha(\lambda)\pi}{\sqrt{\kappa_1\kappa_2}}\int_l^\infty \phi(x)\,\mathrm{d}x, \tag{3.3}$$

where l is the minimum approach distance between the sphere and the plane, $\kappa_1 = \kappa_2 = 1/R$ for the sphere and $\frac{3}{2} \le \alpha \le 2$. The Maugis parameter $\lambda = 2\sigma_0(R/\pi\Delta\gamma K^2)^{1/3}$ describes the transition between the JKR- and DMT-limiting behaviours using an approximate, square force–separation curve of depth σ_0 and integrated area $\Delta\gamma$ [43]. Use of this parameter makes the adhesion properties responsive to changes in the shape of the potential V in a manner that neither the JKR nor DMT solutions can capture individually. The parameter λ also introduces the elastic constants E_i, ν_i of the sphere (1) and surface (2) into the problem through the contact modulus $K = \frac{3}{4}((1-\nu_1^2)/E_1 + (1-\nu_2^2)/E_2)^{-1}$. While there is no analytical expression that relates the prefactor α to λ, there is a simple fit developed by Carpick *et al.* [44] that suffices.

From equation (3.3), we can find the adhesive or 'pull-off' force for the sphere on the layered substrate. Because $F(l) = -\mathrm{d}V/\mathrm{d}l = -\alpha\pi R\phi(l)$ and the bodies are in contact at $l \approx x_0$, we have

$$\begin{aligned} F_{pull\text{-}off}(d) &= -\alpha(\lambda(d))\pi R\phi(x_0, d) \\ &= -\alpha(\lambda(d))\pi R\Delta\gamma(d). \end{aligned} \tag{3.4}$$

This is the typical form for pull-off forces in adhesion problems, but all of the information about the potential in equations (1.1) and (1.2), such as the layer thickness d, is included in a consistent manner. The d-dependence enters into equation (3.4) not only in $\Delta\gamma$, but also in λ as well. Figure 2*c* shows how the pull-off forces will vary with layer thickness d. For large layer thicknesses, the influence of the second term in equation (1.2) on adhesion is negligible and the forces asymptote to the value F_∞. However, in the range of 0.5 nm $\le d \le$ 5 nm, the force is significantly higher.

3.3. Adhesion forces on hydrophobic octadecyltrichlorosilane surfaces

The predicted influence of differences in the thickness of the SiO_2 layer on adhesion forces was observable in drag experiments of setal arrays on the hydrophobic wafers. We performed multiple experiments, consisting of hundreds of individual drag tests, at five different speeds (5, 8.9, 15.8,

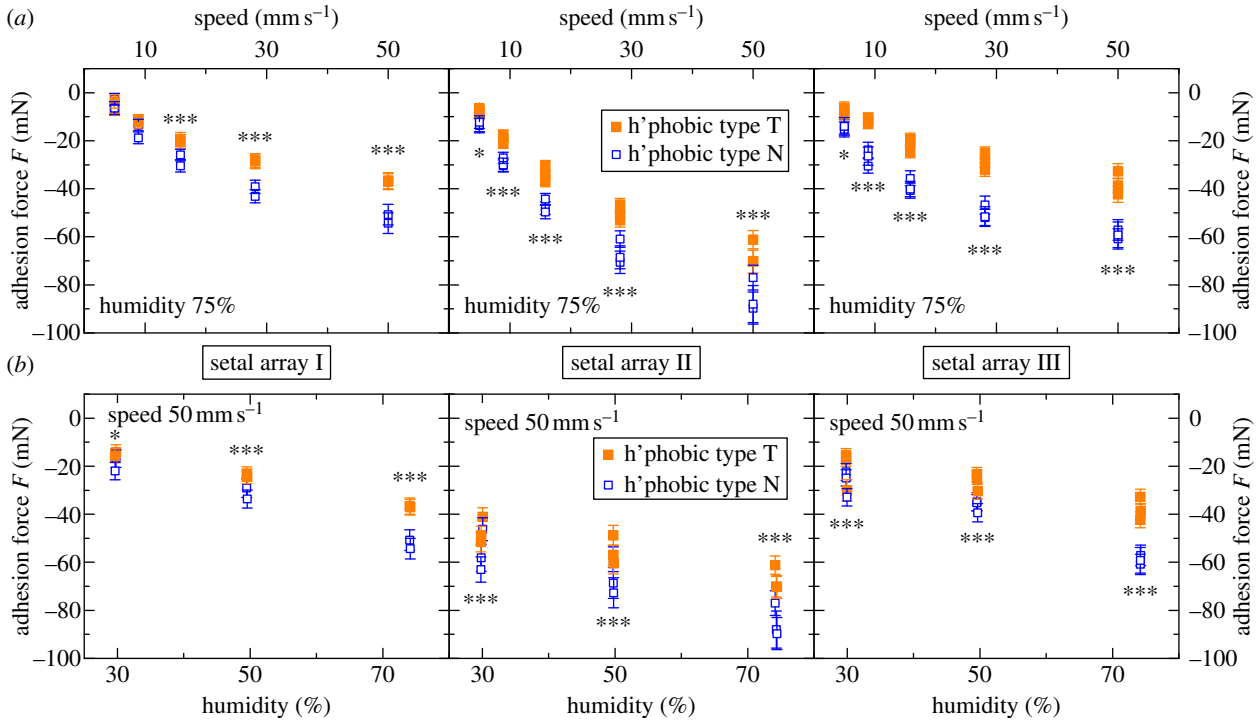

Figure 3. Results of multiple different experiments on the hydrophobic samples with different setal arrays and substrate pairs: mean adhesion forces are plotted as a function of (*a*) the drag speed (at 75% RH) and (*b*) the humidity (with $v = 50$ mm s^{-1}). By convention adhesion forces are negative. The stars indicate the level of significance. (Online version in colour.)

28.1, 50 mm s^{-1}) and three humidities (30%, 50%, 75%RH), incorporating a number of different arrays and substrate pairs. The order of individual tests in an experiment was randomized within the constant-humidity groups. The results of typical experiments are shown in figure 3: the mean adhesion forces of multiple different measurements at 75% RH with different setal arrays and substrate pairs are plotted as a function of drag speed (figure 3*a*) and as a function of humidity (figure 3*b*). The data demonstrate a clear influence of the oxide layer thickness on the adhesion force; the force on the type N substrate is always larger than the force on the type T substrate. The trend is independent of the humidity and the drag speed. Because of the different specimen sizes and slight variations in setal organization between individuals, absolute force values in different experiments depend on the setal array used.

3.4. Adhesion forces on hydrophilic SiO_2 Surfaces

Next, we examined whether the adhesion forces on the bare SiO_2 surfaces are also affected by the SiO_2 layer thickness. Slow drag speeds of 0.5 mm s^{-1} were used to avoid damage to the gecko arrays from the high overall forces on the hydrophilic surfaces.[3] The experiments were performed at four different humidities (10%, 30%, 50%, 70%RH). Similar to the results on the hydrophobic surfaces, the adhesion force on type N wafers is consistently larger than on type T wafers (figure 4*a*). In spite of the slow drag speed, it was not entirely possible to prevent degradation of the array performance during an experiment (no degradation was observed on the hydrophobic samples). To minimize the influence of this effect in our N/T comparisons, we always carried out tests on both substrates in pairs (in a randomized order) and calculated the difference between 'concurrent' N and T measurements. The means of these differences ΔF in various experiments across multiple arrays and substrate pairs are always negative (figure 4*b*). Therefore, the adhesion forces on the bare SiO_2 surfaces are also affected by the SiO_2 layer thickness.

4. Discussion

The experiments demonstrate that the subsurface energy influences macroscopic adhesion. Variation in the oxide layer thickness, which causes subtle differences in the subsurface energy–distance relationship, significantly affects the force of adhesion between gecko setal arrays and Si wafers.

By using two pairs of tailored substrates, we were able to vary subsurface and surface properties independently. On the bare Si/SiO_2 substrates, the adhesion force is higher on the wafers with the thinner SiO_2 layer. This trend in the adhesion force agrees with the theoretical predictions presented in figure 2. Comparing the $F_{\text{pull-off}}(d)$ at $d = 1.7$ nm for the hydrophilic N-type wafer with the value at $d = 151$ nm for the T-type wafer, the pull-off force is—in absolute values—higher on the N-type sample.

On the hydrophobic Si/SiO_2/OTS materials, the overall adhesion force is lower, but the trend corroborates the results on the hydrophilic substrates. To plot $F_{\text{pull-off}}(d)$ for the hydrophobic wafers, it is not necessary to reformulate equation (1.2) with a third layer; rather, the thickness of the OTS layer ($d_{\text{OTS}} \approx 2.6$ nm)[4] is added to that of the SiO_2 layer, because both layers feature similar indexes of refraction and polarizabilities. As the top layer is still on a nanometre scale, the difference in $F_{\text{pull-off}}$ is still resolvable.

It is significant that we can distinguish these slight force differences in an essentially macroscopic experiment with the gecko material. The contact-splitting effect implies that

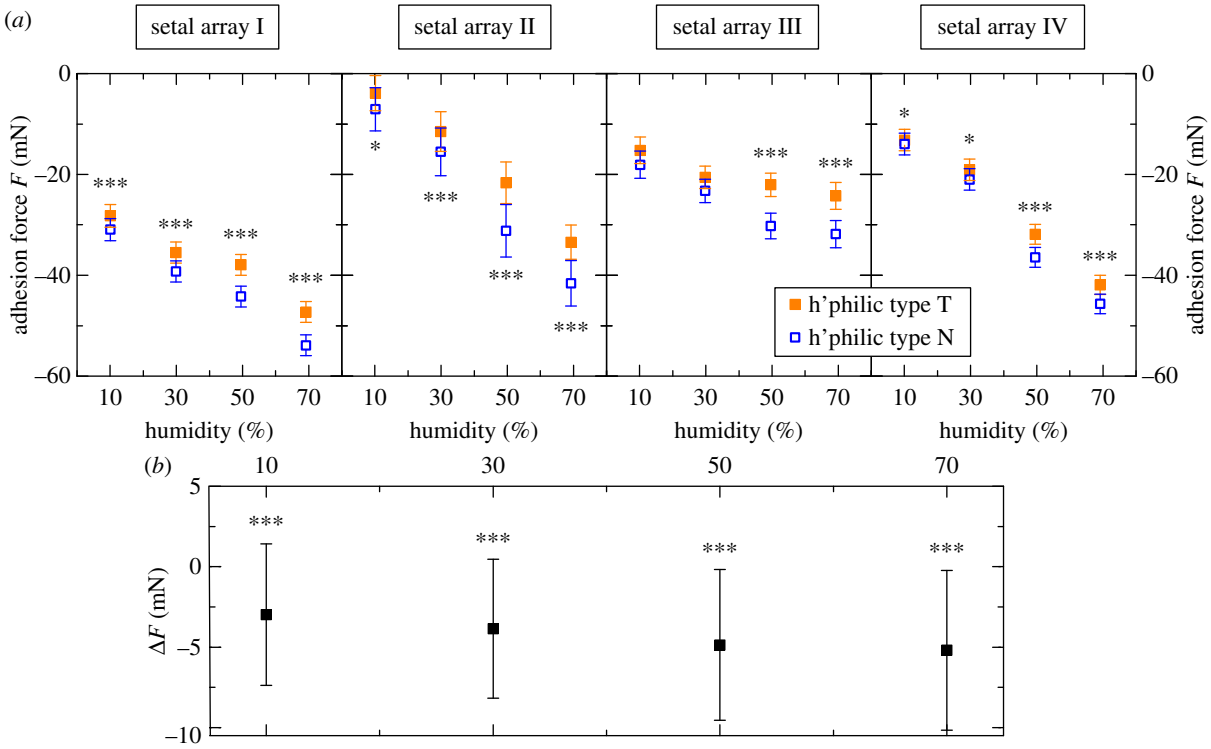

Figure 4. Results of multiple experiments (drag speed: 0.5 mms^{-1}; humidities: 10%, 30%, 50%, 70% RH) on the hydrophilic samples with different setal arrays and substrate pairs: (*a*) mean adhesion forces of the single experiments. (*b*) Aggregation of the experiments on the hydrophilic samples: mean differences in adhesion forces of 'concurrent'; single tests on the type N and type T wafers $\Delta F = F_N - F_T$ are plotted as a function of the humidity. (Online version in colour.)

if we replace a large contact with N smaller ones [45], the overall contact force will be multiplied by a factor of $\sim\sqrt{N}$ [27]. Applying this principle magnifies the slight force differences between the N and T substrates to the point that they can be resolved macroscopically. Tokay geckos possess $\approx$14 000 setae mm^{-2} [46] and there are $\approx$ 100 terminal spatulae on each seta [21].

Furthermore, our data clearly show that adhesion is enforced with increasing drag speed and increasing humidities—on hydrophilic as well as on hydrophobic substrates—corroborating previous studies [25,47,48]. A comparison of the adhesion forces on the hydrophobic and the hydrophilic substrates is not the objective of this study; there are too many variables involved to make any specific inferences. The correlation between water contact angles and gecko adhesion was the focus of previous studies [19,24,49–51].

Our theoretical approximations have two limitations: first, the small size, the internal structure and the unknown optical properties of the wedge-shaped β-keratin pads limit the calculations via the Lifshitz theory, which is based on continuum properties of semi-infinite parallel slabs. However, a more comprehensive and detailed theory will be able to predict more exact values for the subsurface energies of type N and type T wafers, but will not differ from our approximations in the predicted sign of the difference between the surface potentials. Second, the gecko adhesive system does not obey the idealized mechanics of the sphere–plane system. Nevertheless, the JKR/DMT solution includes all of the relevant physical concepts. The variation in the force values in figure 2*c* derives from the difference between the surface potentials ϕ_N and ϕ_T rather than geometrical considerations, and so we expect an analogous response in the gecko system. Thus, we are not able to theoretically match the absolute force values, but we were able to explain the measured differences in adhesion force on type N and type T wafers.

5. Conclusions

By using gecko setae as a macroscopic adhesion probe, we found evidence that differences in the interaction potential associated with the subsurface energy can produce macroscale differences in surface forces. Hence, it is indeed possible to modify the adhesion of materials by stratification. As a consequence, (i) for adhesion and adsorption experiments as well as simulations, vdW forces have to be considered, and (ii) in stratified systems, subsurface and surface energies must be included accordingly.

We are grateful to Jacob Israelachvili for theoretical discussion. We thank Hendrik Hähl and Matthias Lessel for assistance with the substrates as well as Andrew Schnell and Madisen Holbrook for the gecko handling. This work was supported in part by the DAAD PROMOS and the NSF BIO awards (NBM 0900723 and IOS 0847953). P.L., J.P. and M.W. performed the research. P.L. and J.P. analysed data. K.M. gave theoretical advice. K.J. and K.A. designed the research. P.L., J.P., K.J. and K.A. wrote the paper. P.L. and J.P. contributed equally to this work.

Endnotes

[1]Tokay geckos (*Gekko gecko*) can produce an adhesion force of roughly 20 N [17].
[2]In this study, only separations of a few nanometres are of interest. Hence, retardation can be neglected.
[3]On the hydrophobic samples, an effect of wear was not observed.
[4]Determined by ellipsometry and X-ray reflectometry.

References

1. Bhushan B. 2002 *Introduction to tribology*, 1st edn. New York, NY: John Wiley & Sons.
2. Good RJ, Girifalco LA. 1960 A theory for estimation of surface and interfacial energies. III. Estimation of surface energies of solids from contact angle data. *J. Phys. Chem.* **64**, 561–565. (doi:10.1021/j100834a012)
3. Israelachvili J. 1991 *Intermolecular and surface forces*, 2nd edn. San Diego, CA: Academic Press.
4. Parsegian VA. 2006 *Van der Waals forces*, 1st edn. New York, NY: Cambridge University Press.
5. Delrio FW, de Boer MP, Knapp JA, Reedy ED, Clews PJ, Dunn ML. 2005 The role of van der Waals forces in adhesion of micromachined surfaces. *Nat. Mater.* **4**, 629–634. (doi:10.1038/nmat1431)
6. Seemann R, Herminghaus S, Jacobs K. 2001 Dewetting patterns and molecular forces: a reconciliation. *Phys. Rev. Lett.* **86**, 5534–5537. (doi:10.1103/PhysRevLett.86.5534)
7. Jacobs K, Seemann R, Herminghaus S. 2008 Stability and dewetting of thin liquid films. In *Polymer thin films* (eds OKC Tsui, TP Russell), pp. 243–265. Singapore: World Scientific.
8. Indekeu J. 1992 Line tension near the wetting transition: results from an interface displacement model. *Physica A* **183**, 439–461. (doi:10.1016/0378-4371(92)90294-Z)
9. Seemann R, Herminghaus S, Neto C, Schlagowski S, Podzimek D, Konrad R, Mantz H, Jacobs K. 2005 Dynamics and structure formation in thin polymer melt films. *J. Phys. Condensed Matter* **17**, S267–S290. (doi:10.1088/0953-8984/17/9/001)
10. Lalatonne Y, Richardi J, Pileni M. 2004 Van der Waals versus dipolar forces controlling mesoscopic organizations of magnetic nanocrystals. *Nat. Mater.* **3**, 121–125. (doi:10.1038/nmat1054)
11. Quinn A, Mantz H, Jacobs K, Bellion M, Santen L. 2008 Protein adsorption kinetics in different surface potentials. *Europhys. Lett.* **81**, 56003. (doi:10.1209/0295-5075/81/56003)
12. Bellion M, Santen L, Mantz H, Hähl H, Nagel AM, Gilow C, Weitenberg C, Schmitt Y, Jacobs K. 2008 Protein adsorption on tailored substrates: long-range forces and conformational changes. *J. Phys. Condensed Matter* **20**, 404226. (doi:10.1088/0953-8984/20/40/404226)
13. Hähl H *et al*. 2012 Subsurface influence on the structure of protein adsorbates revealed by *in situ* X-ray reflectivity. *Langmuir* **28**, 7747–7756. (doi:10.1021/la300850g)
14. Loskill P, Hähl H, Kreis CT, Thewes N, Bischoff M, Herrmann M, Jacobs K. 2012 The influence of the subsurface composition of a material on the adhesion of *Staphylococci*. *Langmuir* **28**, 7242–7248. (doi:10.1021/la3004323)
15. Parsegian VA. 1993 Reconciliation of van der Waals force measurements between phosphatidylcholine bilayers in water and between bilayer-coated mica surfaces. *Langmuir* **9**, 3625–3628. (doi:10.1021/la00036a044)
16. Israelachvili JN, Tabor D. 1972 The measurement of van der Waals dispersion forces in the range 1.5 to 130 nm. *Proc. R. Soc. Lond. A* **331**, 19–38. (doi:10.1098/rspa.1972.0162)
17. Irschick DJ, Austin CC, Petren K, Fisher RN, Losos JB, Ellers O. 1996 A comparative analysis of clinging ability among pad-bearing lizards. *Biol. J. Linn. Soc.* **59**, 21–35. (doi:10.1111/j.1095-8312.1996.tb01451.x)
18. Geim AK, Dubonos SV, Grigorieva IV, Novoselov KS, Zhukov AA, Shapoval SY. 2003 Microfabricated adhesive mimicking gecko foot-hair. *Nat. Mater.* **2**, 461–463. (doi:10.1038/nmat917)
19. Hiller U. 1968 Untersuchungen zum Feinbau und zur Funktion der Haftborsten von Reptilien. *Z. Morph. Tiere* **62**, 307–362. (doi:10.1007/BF00401561)
20. Ruibal R, Ernst V. 1965 The structure of the digital setae of lizards. *J. Morphol.* **117**, 271–293. (doi:10.1002/jmor.1051170302)
21. Rizzo NW, Gardner KH, Walls DJ, Keiper-Hrynko NM, Ganzke TS, Hallahan DL. 2006 Characterization of the structure and composition of gecko adhesive setae. *J. R. Soc. Interface* **3**, 441–451. (doi:10.1098/rsif.2005.0097)
22. Autumn K, Majidi C, Groff RE, Dittmore A, Fearing R. 2006 Effective elastic modulus of isolated gecko setal arrays. *J. Exp. Biol.* **209**, 3558–3568. (doi:10.1242/jeb.02469)
23. Autumn K, Liang Y, Hsieh ST, Zesch W, Chan W, Kenny T, Fearing RS, Full R. 2000 Adhesive force of a single gecko foot-hair. *Nature* **405**, 681–685. (doi:10.1038/35015073)
24. Autumn K, Peattie AM. 2002 Mechanisms of adhesion in geckos. *Integr. Comp. Biol.* **42**, 1081–1090. (doi:10.1093/icb/42.6.1081)
25. Huber G, Mantz H, Spolenak R, Mecke K, Jacobs K, Gorb SN, Arzt E. 2005 Evidence for capillarity contributions to gecko adhesion from single spatula nanomechanical measurements. *Proc. Natl Acad. Sci. USA* **102**, 16 293–16 296. (doi:10.1073/pnas.0506328102)
26. Loskill P, Hähl H, Faidt T, Grandthyll S, Müller F, Jacobs K. 2012 Is adhesion superficial? Silicon wafers as a model system to study van der Waals interactions. *Adv. Colloid Interface Sci.* **179–182**, 107–113. (doi:10.1016/j.cis.2012.06.006)
27. Arzt E, Gorb S, Spolenak R. 2003 From micro to nano contacts in biological attachment devices. *Proc. Natl Acad Sci. USA* **100**, 10 603–10 606. (doi:10.1073/pnas.1534701100)
28. Lifshitz EM. 1956 The theory of molecular attractive forces between solids. *Sov. Phys. JETP* **2**, 73–83.
29. Dzyaloshinskii IE, Lifshitz EM, Pitaevskii LP. 1961 The general theory of van der Waals forces. *Adv. Phys.* **10**, 165–209. (doi:10.1080/00018736100101281)
30. Gravish N, Wilikinson M, Autumn K. 2008 Frictional and elastic energy in gecko adhesive detachment. *J. R. Soc. Interface* **5**, 339–348. (doi:10.1098/rsif.2007.1077)
31. Autumn K, Dittmore A, Santos D, Spenko M, Cutkosky M. 2006 Frictional adhesion: a new angle on gecko attachment. *J. Exp. Biol.* **209**, 3569–3579. (doi:10.1242/jeb.02486)
32. Brzoska JB, Ben Azouz I, Rondelez F. 1994 Silanization of solid substrates: a step toward reproducibility. *Langmuir* **10**, 4367–4373. (doi:10.1021/la00023a072)
33. Wasserman SR, Whitesides GM, Tidswell IM, Ocko BM, Pershan PS, Axe JD. 1989 The structure of self-assembled monolayers of alkylsiloxanes on silicon: a comparison of results from ellipsometry and low-angle x-ray reflectivity. *Int. J. Biol. Macromol.* **111**, 5852–5861.
34. Gutfreund P, Bäumchen O, van der Grinten D, Fetzer R, Maccarini M, Jacobs K, Zabel H, Wolff M. Submitted. Surface correlation affects liquid order and slip in a Newtonian liquid. (http://arxiv.org/abs/1104.0868)
35. Rizvi TZ, Khan MA. 2008 Temperature-dependent dielectric properties of slightly hydrated horn keratin. *Int. J. Biol. Macromol.* **42**, 292–297. (doi:10.1016/j.ijbiomac.2008.01.001)
36. Maeda H. 1989 Water in keratin. piezoelectric, dielectric, and elastic experiments. *Biophys. J.* **56**, 861–868. (doi:10.1016/S0006-3495(89)82732-8)
37. Sze SM, Ng KK. 2006 *Physics of semiconductor devices*, 3rd edn. New York, NY: John Wiley & Sons.
38. Finklea H, Robinson L, Blackburn A, Richter B, Allara D, Bright T. 1986 Formation of an organized monolayer by solution adsorption of octadecyltrichlorosilane on gold: electrochemical properties and structural characterization. *Langmuir* **2**, 239–244. (doi:10.1021/la00068a022)
39. Mykhaylyk TA, Evans SD, Fernyhough CM, Hamley IW, Henderson JR. 2003 Surface energy of ethylene-co-1-butene copolymers determined by contact angle methods. *J. Colloid Interface Sci.* **260**, 234–239. (doi:10.1016/S0021-9797(02)00188-1)
40. Johnson KL, Kendall K, Roberts AD. 1971 Surface energy and the contact of elastic solids. *Proc. R. Soc. Lond. A* **324**, 301–313. (doi:10.1098/rspa.1971.0141)
41. Derjaguin BV, Muller VM, Toporov YP. 1975 Effect of contact deformations on the adhesion of particles. *J. Colloid Interface Sci.* **53**, 314–326. (doi:10.1016/0021-9797(75)90018-1)
42. Maugis D. 2000 *Contact, adhesion and rupture of solids*, 1st edn. Berlin, Germany: Springer.
43. Maugis D. 1992 Adhesion of spheres: the JKR-DMT transition using a Dugdale model. *J. Colloid Interface Sci.* **150**, 243–269. (doi:10.1016/0021-9797(92)90285-T)
44. Carpick RW, Ogletree DF, Salmeron M. 1999 A general equation for fitting contact area and friction

vs load measurements. *J. Colloid Interface Sci.* **211**, 395–400. (doi:10.1006/jcis.1998.6027)

45. Autumn K *et al*. 2002 Evidence for van der Waals adhesion in gecko setae. *Proc. Natl. Acad. Sci. USA* **99**, 12 252–12 256. (doi:10.1073/pnas.192252799)
46. Schleich H, Kästle W. 1986 Ultrastrukturen an Gecko-Zehen (reptilia: sauria: gekkonidae). *Amphibia Reptilia* **7**, 141–166. (doi:10.1163/156853886X00361)
47. Gravish N *et al*. 2010 Rate-dependent frictional adhesion in natural and synthetic gecko setae. *J. R. Soc. Interface* **7**, 259–269. (doi:10.1098/rsif.2009.0133)
48. Niewiarowski PH, Lopez S, Ge L, Hagan E, Dhinojwala A. 2008 Sticky gecko feet: the role of temperature and humidity. *PLoS ONE* **3**, e2192. (doi:10.1371/journal.pone.0002192)
49. Puthoff JB, Prowse MS, Wilkinson M, Autumn K. 2010 Changes in materials properties explain the effects of humidity on gecko adhesion. *J. Exp. Biol.* **213**, 3699–3704. (doi:10.1242/jeb.047654)
50. Chen B, Gao H. 2010 An alternative explanation of the effect of humidity in gecko adhesion: stiffness reduction enhances adhesion on a rough surface. *Int. J. Appl. Mech.* **2**, 1–9. (doi:10.1142/S1758825110000433)
51. Kim Y, Limanto F, Lee DH, Fearing RS, Maboudian R. 2012 Role of counter-substrate surface energy in macroscale friction of nanofiber arrays. *Langmuir* **28**, 2922–2927. (doi:10.1021/la204078z)